

***Ab initio* simulation of Ta₂O₅: A high symmetry ground state phase with application to interface calculation**

Jun-Hui Yuan,¹ Kan-Hao Xue,^{1,*} Qi Chen,¹ Leonardo R. C. Fonseca,² and Xiang-Shui Miao^{1,#}

¹ Wuhan National Research Center for Optoelectronics, School of Optical and Electronic Information, Huazhong University of Science and Technology, Wuhan 430074, China

² Departamento de Física, ICEx, Universidade Federal de Minas Gerais, 30123-970 Belo Horizonte, MG, Brazil

Corresponding Authors

*E-mail: xkh@hust.edu.cn (K.-H. Xue) #E-mail: miaoxs@hust.edu.cn (X.-S. Miao)

ABSTRACT

We suggest a tetragonal $I4_1/amd$ phase (η -phase) as the ground state of Ta₂O₅ at zero temperature, which is a high symmetry version of the triclinic γ -phase Ta₂O₅ predicted by Yang and Kawazoe. Our calculation shows that γ -phase Ta₂O₅ will automatically be transformed into the η -phase during structural relaxation. Phonon dispersion confirms that the η -phase is dynamically stable, while the high temperature α -phase Ta₂O₅, which also has the $I4_1/amd$ symmetry, is unstable at zero temperature. A thorough energy comparison of the β_{AL} , δ , λ , B, L_{SR}, β_R , Pm , $Cmmm$, γ , η and α phases of Ta₂O₅ is carried out. The GGA-1/2 method is applied in calculating the electronic structure of various phases, where the η -phase demonstrates a 4.24 eV indirect band gap, close to experimental value. The high symmetry tetragonal phase together with computationally efficient GGA-1/2 method greatly facilitate the *ab initio* simulation of Ta₂O₅-based devices. As an example, we have explicitly shown the Ohmic contact nature between metal Ta and Ta₂O₅ by calculating an interface model of *b.c.c.* Ta and η -Ta₂O₅, using GGA-1/2.

Key words: η -phase Ta₂O₅, self-energy correction, GGA-1/2, tantalum penta-oxide

I. INTRODUCTION

Tantalum penta-oxide (Ta_2O_5) is a versatile functional dielectric that can be used as electrolytic capacitor,^[1] optical modulator,^[2] optical coating,^[3] high-K dielectric material in microelectronics,^[4] and the switching layer in memristors.^{[5]–[10]} Despite its wide range of applications, the knowledge of its exact structure is nevertheless still limited. At zero temperature, the structure of ground state Ta_2O_5 crystal has been under debate for decades.^{[11]–[13]} On the other hand, the applied computational researches on $\text{Ta}_2\text{O}_5/\text{TaO}_x$ have been much more rare^{[14],[15]} compared with $\text{HfO}_2/\text{HfO}_x$,^{[16]–[27]} though TaO_x and HfO_x share many properties in common and both are regarded as the most promising candidates for next-generation memristors. This state of affairs is strongly related to the uncertainty regarding which model to use for the ground state of Ta_2O_5 . Indeed, most computational works have been still focusing on revealing the ground state atomic structures of Ta_2O_5 .^[13] Furthermore, to correctly describe the electronic structure of various Ta_2O_5 phases remains a challenging task, where one either accepts the band gap underestimation stemming from the local density approximation^[28] (LDA) and generalized gradient approximation^{[29],[30]} (GGA) of density functional theory^[31] (DFT), or has to resort to hybrid functionals^[32] and quasi-particle approaches such as the GW approximation.^[33] Although Cui and Jiang obtained excellent GW electronic structures for Ta_2O_5 ,^[34] the computational load is formidable when large supercells involving interfaces and point defects are considered. In order to investigate complex structures at the device level, it is necessary to develop a more efficient methodology

for the theoretical simulation of large Ta₂O₅-based supercells involving hundreds of atoms.

A comparison with HfO₂ further clarifies the difficulty regarding the electronic structure calculation for Ta₂O₅. While DFT-LDA and DFT-GGA also severely underestimate the band gap of HfO₂, the more accurate G_0W_0 method reveals relatively uniform band gap values among its various phases, such as monoclinic ($P2_1/c$, 5.45 eV), tetragonal ($P4_2/nmc$, 5.78 eV), and cubic ($Fm\bar{3}m$, 4.91 eV),^[35] thus one may calculate any hafnia system using conventional GGA while the true band gap can readily be estimated with good reliability. On the contrary, the calculated band gap values for various Ta₂O₅ phases differ a lot. For instance, using GW approximation Lee *et al.* reported 1.03 eV, 2.22 eV, 2.96 eV and 4.26 eV band gaps for β -Ta₂O₅ ($Pccm$), δ -Ta₂O₅, orthorhombic Ta₂₂O₅₅ and amorphous Ta₂O₅, respectively.^[36] Moreover, while the primitive cells of various HfO₂ phases contain few atoms, typically not more than 12, many models for Ta₂O₅ require large primitive cells, even containing 77 atoms in the famous model of Stephenson and Roth.^[11] Very recently, Yang and Kawazoe proposed a new triclinic phase for Ta₂O₅,^[13] whose energy is lower than any other proposed Ta₂O₅ models. However, due to the lack of symmetry, its adoption in interfacial models is quite challenging.

In this work, we suggest a tetragonal $I4_1/amd$ phase (referred to as η phase) as a prototype ground state of Ta₂O₅, which can be regarded as a high symmetry counterpart

of the triclinic structure proposed by Yang and Kawazoe. The self-energy corrected LDA-1/2 and GGA-1/2 methods (referred to as DFT-1/2 in general) are utilized to calculate the electronic structures of η -Ta₂O₅, recovering band gaps close to experimental value. The new high symmetry phase and the efficient DFT-1/2 method can be combined to investigate several practical issues relevant to Ta₂O₅-based devices.

II. COMPUTATIONAL

Existing model structures for Ta₂O₅

As our aim is to identify the most suitable Ta₂O₅ phase for ground state density functional calculations, we shall focus here on the low temperature phases of Ta₂O₅ (L-Ta₂O₅). Yet, knowledge of the high temperature phases is still valuable since they are usually more symmetric. Above 1360°C,^[37] Ta₂O₅ is in the high temperature phase named H-Ta₂O₅ or α -Ta₂O₅, for which various model structures have been proposed including triclinic, monoclinic, orthorhombic and tetragonal structures.^{[38],[39]} Fortunately, the most symmetric tetragonal phase has been fully refined, in an $I4_1/amd$ symmetry.^[39]

For L-Ta₂O₅, early in the 1960s, hexagonal (named δ -Ta₂O₅ or TT-Ta₂O₅), monoclinic and orthorhombic (usually referred to as β -Ta₂O₅) phases of L-Ta₂O₅ were already reported experimentally.^{[40]-[42]} Based on X-ray diffraction (XRD) patterns, Stephenson and Roth initially proposed an orthorhombic model for L-Ta₂O₅ in 1971, with a unit cell of Ta₂₂O₅₅.^[11] This model, usually named as the L_{SR} model in the literature, contains

a certain amount of oxygen vacancies to reach the Ta_2O_5 stoichiometry. Several years later, a high pressure phase of L- Ta_2O_5 was discovered by Izumi and Kodama through hydrothermal synthesis,^[43] referred to as B- Ta_2O_5 . It is isomorphic with the B- Nb_2O_5 , both possessing a monoclinic $C2/c$ structure. However, B- Ta_2O_5 was found to be stable even at atmospheric pressure and low temperature.^{[43],[44]} In 1992, Hummel *et al.* identified the space group of δ - Ta_2O_5 as $P6/mmm$, but the exact atomic structure was still unknown.^[45] Meanwhile, starting from δ - Ta_2O_5 they also synthesized a new single crystal phase of Ta_2O_5 , the so-called T- Ta_2O_5 with an orthorhombic $Pmm2$ symmetry. The exact structure was identified, which actually has the non-stoichiometric $\text{Ta}_{24}\text{O}_{62}$ composition.^[45] Later in 1997, Fukumoto and Miwa identified the exact atomic structure of δ - Ta_2O_5 using first-principles calculations,^[46] which has a Ta_4O_{10} unit cell with the $P6/mmm$ symmetry.

Research into the atomic structure of L- Ta_2O_5 has been very intensive in recent years, due to the importance of Ta_2O_5 in microelectronics. Sawada and Kawakami proposed a simplified Ta_6O_{15} model supercell instead of the L_{RS} model in 1999,^[47] so as to facilitate the simulation. This model relaxes to a monoclinic structure with Pm symmetry in our calculation. Through Rietveld full-profile analysis on the XRD patterns, Aleshina and Loginova obtained a $Pccm$ model structure for orthorhombic L- Ta_2O_5 in 2002,^[48] denoted as the β_{AL} phase. Shortly after that, Ramprasad proposed another orthorhombic model with a Ta_4O_{10} unit cell (denoted as β_R model in the literature),^[49] which was an simplified version of the L_{SR} model for the sake of simulation efficiency. The original

β_R model has a Pm symmetry, but after relaxation it becomes a more symmetric $Pmma$ phase in our calculation. In 2005, Grey *et al.* synthesized a new phase of single crystal L-Ta₂O₅ in the monoclinic $C2/m$ symmetry, whose unit cell composition is Ta₃₈O₉₅. In 2013, Lee *et al.* predicted a high symmetry $Pbam$ phase for orthorhombic Ta₂O₅ with a simple Ta₄O₁₀ unit cell, which is called λ -Ta₂O₅.^[50] The energy of λ -Ta₂O₅ is, according to the original calculation, lower than the L_{SR} model, but it remained uncertain whether it is the most suitable ground state for L-Ta₂O₅. Later, an orthorhombic $Cmmm$ structure was proposed by Kim *et al.* in 2014,^[51] which is energetically more favorable than λ -Ta₂O₅ according to their calculation.

Most recently, Yang and Kawazoe identified a triclinic phase of Ta₂O₅ using *ab initio* evolutionary algorithm, as a new ground state for L-Ta₂O₅.^[13] Named as γ -Ta₂O₅, this phase was reported to be considerably more stable than any other known phase of Ta₂O₅ at zero temperature and atmospheric pressure, though the $Cmmm$ -phase Ta₂O₅ was not explicitly listed in their comparison. The discovery of the γ -phase can be regarded as a great success of modern structural prediction methodology by combining density functional theory and the evolutionary algorithm. Yet, the triclinic nature of this phase may impose certain difficulties in model construction for Ta₂O₅-related interfaces and capacitors. Therefore, it is still worthwhile to develop a simple orthorhombic (or even more symmetric) phase for L-Ta₂O₅, whose energy is lower than λ -Ta₂O₅ and close to γ -Ta₂O₅.

Fundamental computational settings

DFT calculations were carried out using the plane-wave-based Vienna *Ab initio* Simulation Package,^{[52],[53]} with a fixed 500 eV plane-wave kinetic energy cutoff. For the exchange-correlation (XC) energy, three distinct functionals were considered: the LDA functional of Ceperley-Alder^[54] parameterized by Perdew and Zunger^[55] (CA), the GGA functional of Perdew-Burke-Ernzerhof (PBE),^[30] and the PBEsol functional that was specially designed for solids.^[56] The electrons considered as valence were: $5p$, $5d$ and $6s$ for Ta; $2s$ and $2p$ for O. Core electrons were approximated by projector augmented-wave pseudopotentials.^{[57],[58]} In all self-consistent runs, the convergence criterion for total energy was 10^{-6} eV, while structural optimization was reached for Hellmann-Feynman forces on any atom less than 0.01 eV/Å in each direction.

DFT-1/2 for improved band structures

The band gap underestimation by DFT-LDA and DFT-GGA has long been a well-known problem,^[59] which is attributed to the lacking of derivative discontinuity in the XC functionals.^{[60],[61]} The DFT-1/2 method, proposed by Ferreira *et al.* in 2008,^[62] attributed the band gap underestimation to a self-energy term of the valence band hole in the intrinsic excitation of a semiconductor. The subtraction of this self-energy rectifies the band gap, but DFT-1/2 does such correction within the Kohn-Sham framework, unlike the *GW* approximation that goes beyond.

In practice, one does not calculate the self-energy of the hole using perturbative methods. Rather, since the hole is localized near the anions, one simply attaches the corresponding “self-energy potential” V_S to these anions (usually summed to the pseudopotential) in real space. The self-energy correction is achieved after a second self-consistent calculation using the self-energy corrected pseudopotential. To keep the self-energy potential local to the corresponding anion, it must be trimmed before summing to anion pseudopotential. The optimal cutoff radius is obtained variationally by maximizing the band gap. Because the self-energy potentials are introduced in the solid state calculations as external atomic potentials, the ground state energies given by DFT-1/2 self-consistent calculations are not physically meaningful. Nevertheless, electronic band diagrams and density of states are properly corrected by DFT-1/2.^[62] Hence, in our work all total energies were taken from DFT calculations, while the band diagrams were obtained from either DFT or DFT-1/2 calculations.

Since Ta_2O_5 is a binary metal oxide, the self-energy correction ought to be carried out only for the oxygen anions. The optimal cutoff radius to trim the corresponding V_S (with half electron subtracted from the O 2p orbital^[62]) was obtained variationally upon maximizing the band gap,^[62] and no empirical parameters were involved.

The oxygen self-energy potentials specific to all these XC functionals (LDA-CA, GGA-PBE, GGA-PBEsol) were derived from atomic calculations using a modified ATOM code (supplied with the Siesta simulation package^[63]). We have also created a web-

based self-energy correction program, where pseudopotentials modified by the inclusion of DFT-1/2 self-energy potentials can be generated online for all these XC functionals.^[64]

III. RESULTS AND DISCUSSIONS

Optimized crystal structures of previously identified L-Ta₂O₅ phases

We studied in detail nine representative L-Ta₂O₅ phases, as shown in **Figure 1**. The *Pmm2* phase was not considered because it is non-stoichiometric, while the *C2/m* phase was omitted because of its rather complex unit cell (Ta₃₈O₉₅). In addition, the high temperature α -phase was also included for comparison. The optimized lattice parameters for these ten structures are summarized in **Table 1**, together with the corresponding theoretical and experimental values in the literature.

Table 1 Calculated structural parameters for L-Ta₂O₅ in β_{AL} , δ , λ , B, L_{SR}, β_R , *Pm*, *Cmmm*, γ and α phases using various XC functionals. Previous reported theoretical and experimental values are listed for comparison. In parenthesis we indicate the relative error with respect to the experimental value.

	LDA	PBE	PBEsol	Literature	
				Theory	Expt.
β_{AL} -phase					
a (Å)	6.371(+2.45%)	6.511(+4.71%)	6.424(+3.33%)	6.52 ^[13]	6.217 ^[48]
b (Å)	3.658(-0.52%)	3.698(+0.57%)	3.676(-0.03%)	3.69	3.677
c (Å)	7.691(-1.32%)	7.778(-0.21%)	7.728(-0.85%)	7.78	7.794
δ -phase					
a (Å)	7.215(-0.34%)	7.338(+1.35%)	7.267(+0.37%)	7.33 ^[13]	7.24 ^[41]
c (Å)	3.845(-0.90%)	3.888(-0.21%)	3.863(-0.44%)	3.89	3.88
γ angle (°)	120	120	120	120	

			λ -phase		
a (Å)	6.160	6.258	6.199	6.25 ^[13]	
b (Å)	7.270	7.412	7.332	7.40	
c (Å)	3.770	3.826	3.795	3.82	
			B-phase		
a (Å)	12.759(-0.20%)	12.941(+1.22%)	12.834(+0.38%)	12.93 ^[13]	12.785 ^[65]
b (Å)	4.824(-0.62%)	4.922(+1.40%)	4.867(+0.27%)	4.92	4.854
c (Å)	5.484(-0.80%)	5.593(+1.17%)	5.528(0.00%)	5.59	5.528
β angle (°)	104.22(-0.04%)	103.20(-1.02%)	103.77(-0.47%)	103.23	104.26
			L_{SR} -phase		
a (Å)	6.230 (+0.52%)	6.336 (+2.23%)	6.274 (+1.23%)	6.33 ^[13]	6.198 ^[11]
b (Å)	40.223 (-0.17%)	41.058 (+1.91%)	40.627 (-0.84%)	40.92	40.290
c (Å)	3.787 (-2.60%)	3.843 (-1.16%)	3.812 (-1.95%)	3.85	3.888
γ angle (°)	90.12 (+0.13%)	90.13 (+0.14%)	89.97 (-0.03%)	89.16	90
			β_R -phase		
a (Å)	6.141	6.221	6.173	6.03 ^[49]	
b (Å)	7.244	7.431	7.322	7.13	
c (Å)	3.831	3.874	3.850	3.82	
			Pm -Ta ₆ O ₁₅		
a (Å)	6.241	6.372	6.295		
b (Å)	3.759	3.822	3.789		
c (Å)	11.058	11.246	11.139		
β angle (°)	87.95	87.32	87.61		
			$Cmmm$ -phase		
a (Å)	3.818	3.871	3.845	3.79 ^[51]	
b (Å)	12.937	13.146	13.018	12.79	
c (Å)	3.845	3.891	3.865	3.81	
			γ -phase		
a (Å)	3.836	3.883	3.858	3.89 ^[13]	
b (Å)	3.835	3.884	3.858	3.89	
c (Å)	13.209	13.421	13.294	13.38	
α angle (°)	81.708	81.710	81.645	81.77	
β angle (°)	98.349	98.336	98.332	98.25	
γ angle (°)	90.001	90.001	90.000	89.67	
			α -phase		
a (Å)	3.893 (+0.85%)	3.872 (+0.31%)	3.834 (-0.67%)	3.85 ^[66]	3.86 ^[39]
c (Å)	36.450 (+0.75%)	36.573 (+1.09%)	36.031 (-0.41%)	37.45	36.18

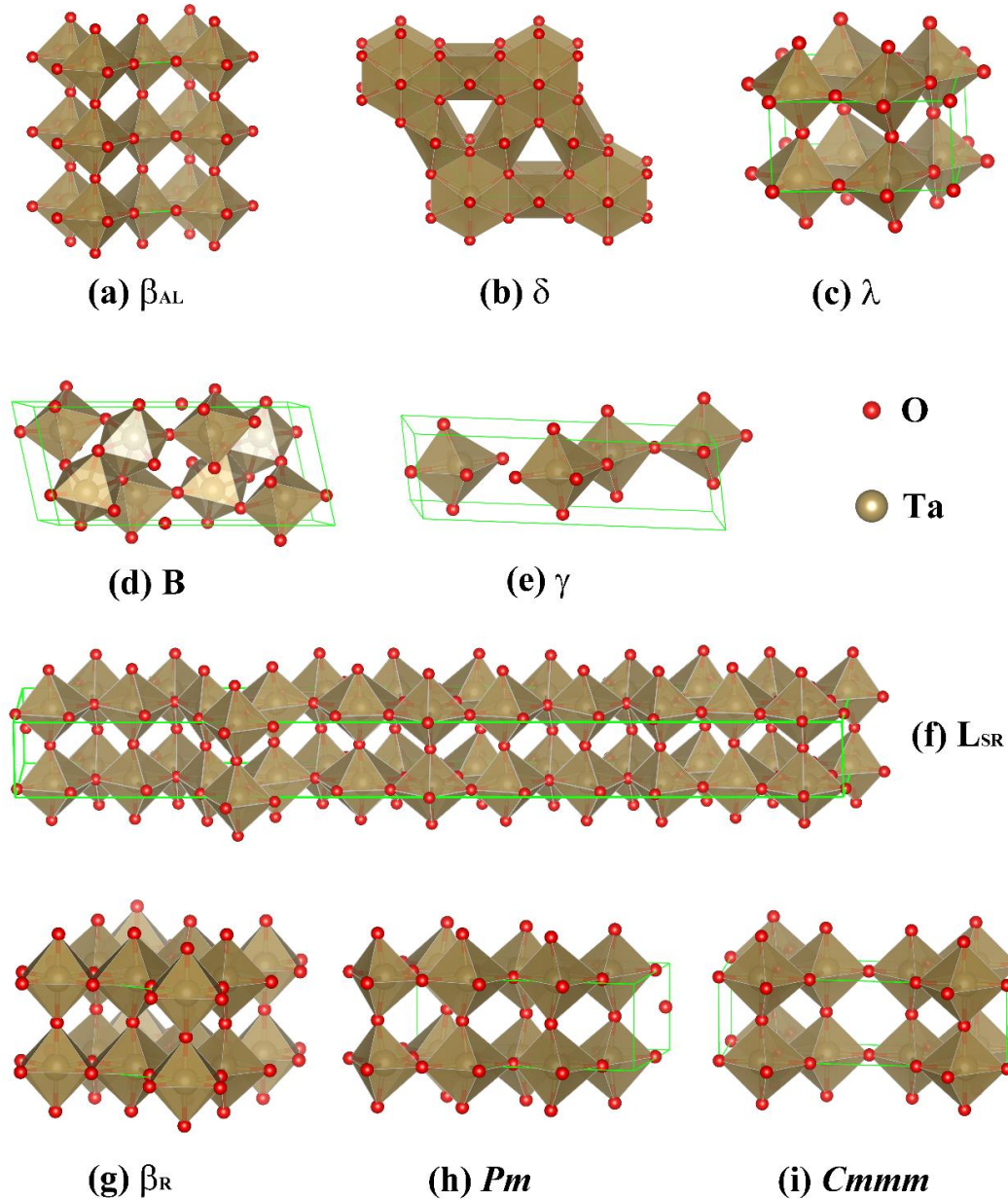


Figure 1. Crystal structures of various Ta₂O₅ models/phases: (a) β_{AL} , (b) δ , (c) λ , (d) B, (e) γ , (f) L_{SR}, (g) β_R , (h) Pm , and (i) $Cmmm$.

Our results are in general consistent with the data reported in the literature, with the γ -phase as the only exception. While the exact space group was not given in the original work, the structural data literally point to a $P1$ space group with the lowest symmetry. We thus carried out structural relaxations on the γ -phase Ta₂O₅ in the $P1$ symmetry.

Remarkably, our γ angle is 90° within the computational error range, regardless of the XC functional used. This implies that the γ phase may in fact possess higher symmetry which makes it worthwhile to carry out an in-depth investigation of this issue.

A high-symmetry model structure for the ground state of L-Ta₂O₅

As discussed above, our optimization of the γ -phase accompanies a change of the γ -angle from 89.67° in the original work^[13] to 90.00° in the present work. Since the total energy gets lower during structural relaxation, this implies that the true ground state can be assigned a more symmetric space group. Confined to the *P1* (No. 1) symmetry, we had missed certain symmetry elements because no calculation could yield absolute accuracy. A careful inspection on our relaxed “ γ -phase” led to a much higher symmetry in the space group *I4₁/amd* (No. 141), whose full structural data are listed in **Table 2**.

Table 2 Structural parameters of η -Ta₂O₅ in the *I4₁/amd* symmetry.

	<i>Space group</i>			<i>a</i> (Å)	<i>c</i> (Å)
η -Ta ₂ O ₅	<i>I4₁/amd</i>			3.883	26.272
<i>Sites</i>	<i>x</i>	<i>y</i>	<i>z</i>	<i>Wyckoff position</i>	
Ta 1	0	0	0.0729	8e	
O 1	0	0	0	4a	
O 2	0	0	0.1570	8e	
O 3	0	0	0.6769	8e	

Since the γ -phase was already assigned the triclinic symmetry, we here refer to this high symmetry *I4₁/amd* phase as η -phase. To demonstrate their relations, in **Figures 2(a)**

and **2(b)** we plot $3 \times 3 \times 3$ supercells of the γ -phase and the η -phase for comparison. First we notice that the a and b axes are orthogonal in the η -phase, but not in the γ -phase. Secondly, the marked O-Ta-O bond angle (highlighted in **Figure 2(a)**) along the b -axis is 171.5° in γ -Ta₂O₅, while in η -Ta₂O₅ it is 180.0° . The high symmetry of the η -phase is not clear when viewed along the c -direction (**Figure 2(c)**), because the c -axis is not orthogonal to the a - b plane. Yet, the tetragonal symmetry is manifested when viewing along the z -direction, which is exactly the direction orthogonal to the a - b plane (**Figure 2(d)**).

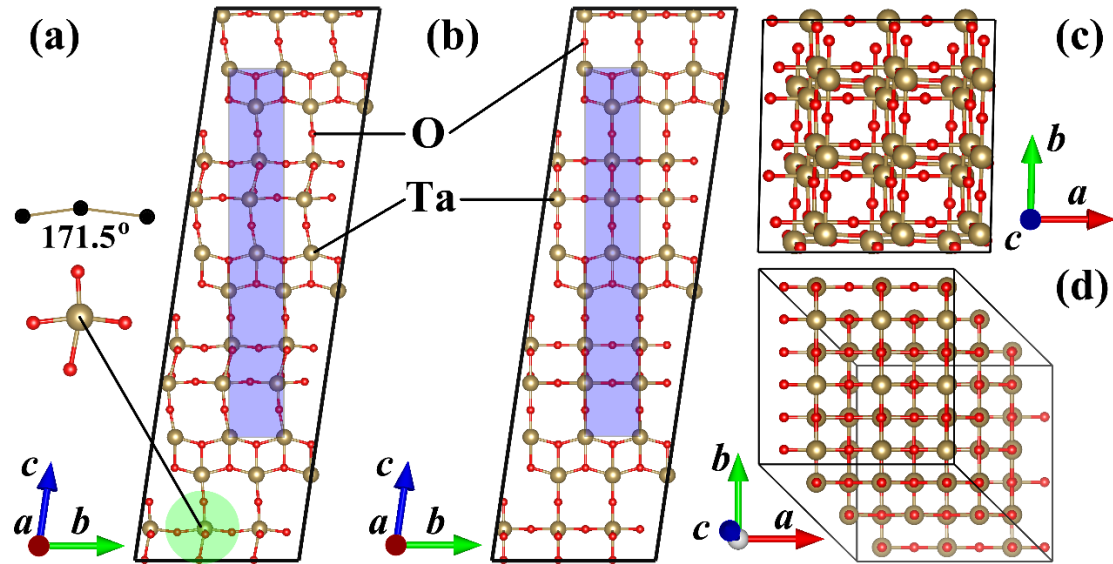


Figure 2. (a) Atomic structure of the original γ -phase Ta₂O₅; (b) fully relaxed “ γ -phase” in our calculation, viewed along the a -axis; (c) view of the structure in (b) along the c -axis; (d) view of the structure in (b) along z -axis, which is orthogonal to the a - b plane.

The tetragonal unit cell of η -Ta₂O₅ can be extracted from the rectangular shaded region in **Figure 2(b)**. Interestingly, the most widely accepted phase of H-Ta₂O₅ (α -Ta₂O₅) also has the $I4_1/amd$ symmetry. It is a very unusual situation that the zero temperature phase and the high temperature phase share the same space group. Therefore, we make

a structural comparison of the $I4_1/amd$ L-Ta₂O₅ and $I4_1/amd$ H-Ta₂O₅ in **Figure 3**. The α -Ta₂O₅ structure is more complicated in that it involves fractional (75%) occupation O sites. Besides, the Ta-O bonds in η -Ta₂O₅ mainly extend along a -, b - and c -axes, with only slight distortions in certain regions. Nevertheless, the Ta-O-Ta bonds at the fractional occupation O sites make big angles with the axes, on the a - b and a - c planes. The existence of oxygen vacancies in α -Ta₂O₅ reduces the Gibbs free energy through the entropy-related term at finite temperatures.

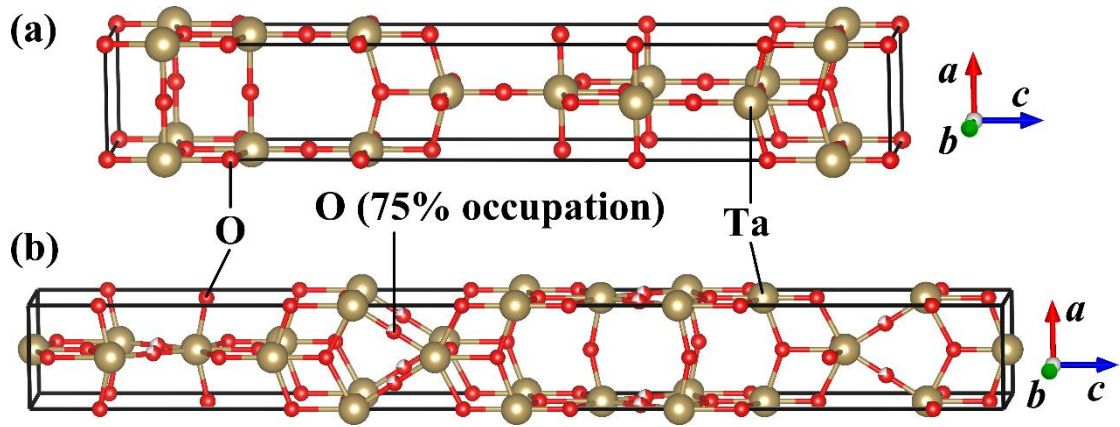


Figure 3. (a) Atomic structure of the $I4_1/amd$ η -phase Ta₂O₅; (b) atomic structure of the $I4_1/amd$ H-Ta₂O₅ (α -Ta₂O₅).

Since the γ -phase automatically transforms into the η -phase in our structural optimization, we compared the energies of the two phases in a special way. We fixed the shape of γ -Ta₂O₅ to the original settings of Yang and Kawazoe,^[13] and optimized the cell volume and atomic coordinates, in order to keep the triclinic symmetry. In this way we find that the η -phase is energetically lower than the γ -phase by 0.0016 eV per Ta₂O₅ chemical formula. Compared with other phases, we confirm that the η -phase has the lowest energy among various Ta₂O₅ models at zero temperature, where the relative

energetics obtained with GGA(PBE) are indicated in **Figure 4**. The reference zero energy was taken as that of the relaxed a-Ta₂O₅ model shown in **Figure 5(a)**. The energetics results indicate that most of the recently proposed orthorhombic (or with slight monoclinic distortion in the case of *Pm* phase) models are lower in energy than the amorphous phase. Actually, the arrangement of the Ta-O octahedra is very similar among L_{SR}, β_R, *Pm* and *Cmmm* phases, as seen in **Figure 1**. The two lowest energy phases are obviously the η-phase and the γ-phase. The *Cmmm* phase is the third lowest one in energy, whose energy per Ta₂O₅ formula is higher than the η-phase by merely 0.09 eV. Finally, we notice that the high temperature α-Ta₂O₅ phase is slightly higher in energy than the amorphous phase, by 0.17 eV per Ta₂O₅ formula.

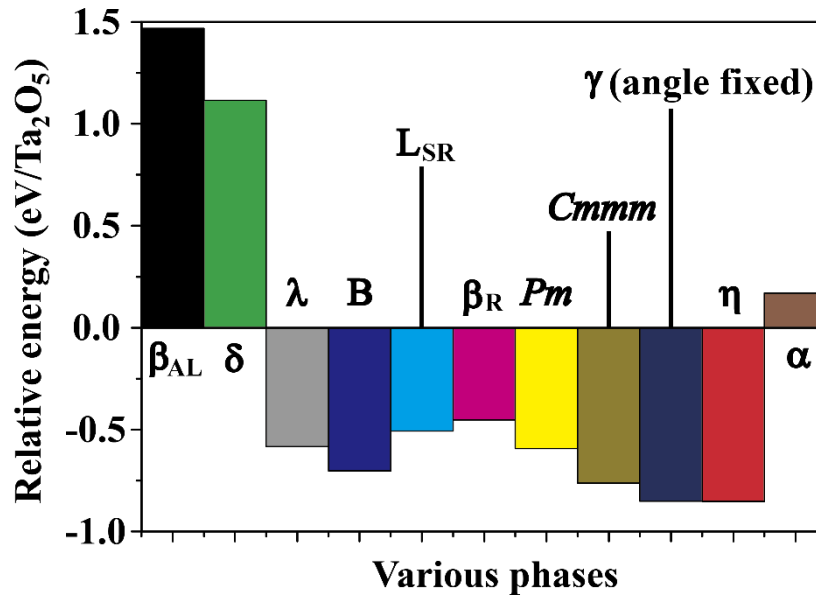


Figure 4. Relative energies per unit formula for Ta₂O₅ in various phases, calculated using GGA(PBE). The energy of the amorphous phase (a-Ta₂O₅) is set to zero.

The dynamic stability of η-Ta₂O₅ was examined through its phonon spectra. As shown in **Figure 6**, no imaginary frequency modes are observed, indicating dynamic

robustness. Due to its high symmetry, low energy and dynamically stable nature, η - Ta_2O_5 is highly recommended as the ground state phase to be used in *ab initio* simulation for Ta_2O_5 .

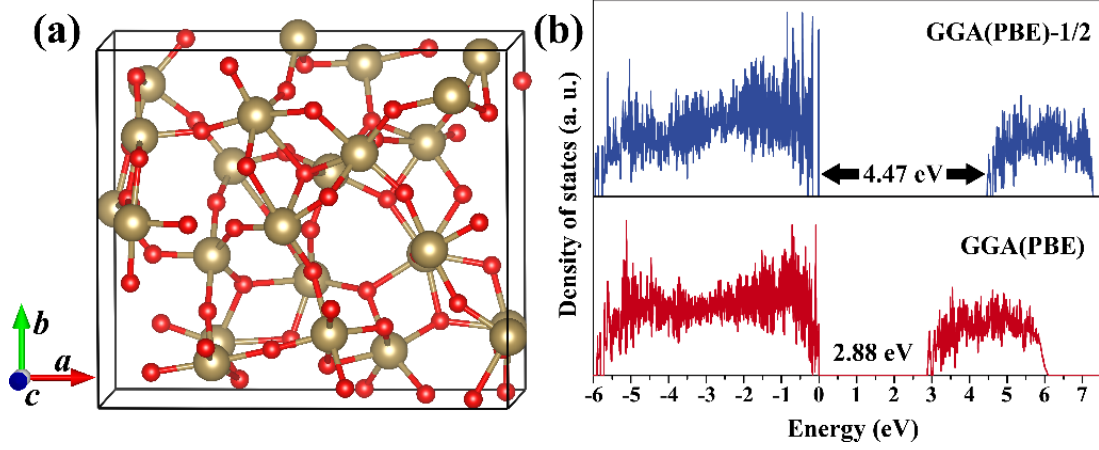


Figure 5. (a) Our optimized amorphous Ta_2O_5 (a- Ta_2O_5) model; (b) its density of states calculated by GGA(PBE) and GGA(PBE)-1/2.

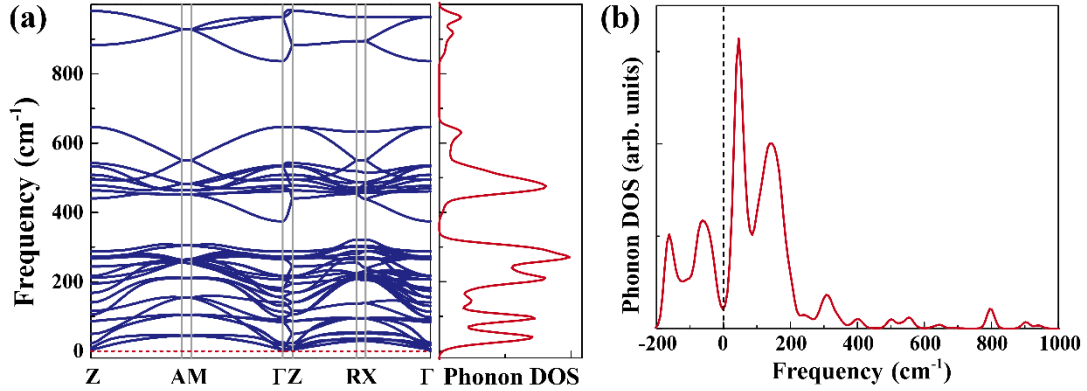


Figure 6. (a) Calculated phonon dispersion and phonon density of states of η - Ta_2O_5 at zero temperature; (b) calculated phonon density of states of α - Ta_2O_5 (H- Ta_2O_5) at zero temperature.

We finally note that η - Ta_2O_5 is actually isomorphic to the tetragonal phase P- Nb_2O_5 , whose structure was first revealed by Petter and Laves in 1965,^[67] with $a = 3.90 \text{ \AA}$ and $c = 25.43 \text{ \AA}$. Initially, Petter and Laves named this phase η - Nb_2O_5 , therefore we refer

to the $I4_1/amd$ phase of Ta_2O_5 as η - Ta_2O_5 following this convention. Yet, researches on η - Nb_2O_5 have been rare compared with the more ordinary form of monoclinic H - Nb_2O_5 . Laves, Moser and Petter observed the similarity of η - Nb_2O_5 to α - Ta_2O_5 , and suggested that the space group of η - Nb_2O_5 may be $I4_1$ or $I4_122$.^[68] Several later works by Valencia-Balvín *et al.*^[69] and Xu *et al.*^[70] assigned the space group $I4_122$ (No. 98, point group D_4) to η - Nb_2O_5 . However, our calculation reveals that the prototype η - Nb_2O_5 has the D_{4h} point group and belongs to a higher symmetry space group $I4_1/amd$, identical to that of η - Ta_2O_5 .

Electronic structures of η - Ta_2O_5 with comparison to other phases

The experimental band gap value of L - Ta_2O_5 ranges from 3.9 eV to 4.5 eV,^{[71]–[73]} usually measured in thin film format where the band gap can be larger than in the bulk. A reasonable calculated band gap value for bulk L - Ta_2O_5 should be slightly greater than 4 eV. Our calculated band gap for a - Ta_2O_5 , which typically possesses larger band gap than crystalline phases, is 2.88 eV using GGA(PBE) (lower part of **Figure 5(b)**). Such severe underestimation is expected due to the missing of self-energy correction. To carry out self-energy correction using GGA-1/2, we attached the trimmed self-energy potential of oxygen to a - Ta_2O_5 , using various cutoff radii with a power index of 20 in the cutoff function.^[64] The optimum cutoff radius was fixed to be 2.3 bohr through a variation process, which eventually maximized the band gap. The corresponding electronic density of states for a - Ta_2O_5 , as shown in the upper part of **Figure 5(b)**, yields a GGA-1/2 band gap of 4.47 eV, which is consistent with the experimental values for

a-Ta₂O₅ (4.2 eV to 4.5 eV^[73]).

Table 2 Calculated DFT and DFT-1/2 band gaps (eV) for (from top to bottom) β_{AL} , δ , λ , B, L_{SR}, β_R , Pm , $Cmmm$, γ (relaxed) and η phases of Ta₂O₅, with different exchange-correlation potentials and optimized lattice parameters. Some theoretical and experimental values are listed for comparison.

	This work			Literature		
	LDA-CA	GGA-PBE	GGA-PBEsol	Hybrid functionals	<i>GW</i>	Expt.
β_{AL} phase						
DFT	0.23(<i>i</i>)	0.26(<i>i</i>)	0.25(<i>i</i>)	1.52 ^{*[74]}	1.81,	3.9 ^[71] , 4.2 ^[72]
DFT-1/2	1.81(<i>i</i>)	1.85(<i>i</i>)	1.85(<i>i</i>)	~2 ^[75] , 2.45 ^{&[76]}	2.42 ^[74]	4.5 ^[73]
				1.70 ^{#[77]}	1.03 ^[78]	
δ phase						
DFT	1.23(<i>i</i>)	1.12(<i>i</i>)	1.20(<i>i</i>)	~2 ^[75] , 2.92 ^{&[76]}	2.22 ^[78]	3.9 ^[71] , 4.2 ^[72]
DFT-1/2	2.79(<i>i</i>)	2.56(<i>i</i>)	2.73(<i>i</i>)	2.87 ^{#[77]}		4.5 ^[73]
λ phase						
DFT	2.07(<i>d</i>)	2.13(<i>d</i>)	2.10(<i>d</i>)	~4.0 ^[75]		3.9 ^[71] , 4.2 ^[72]
DFT-1/2	4.00(<i>d</i>)	4.09(<i>d</i>)	4.06(<i>d</i>)	3.7(<i>d</i>) ^{*[12]}		4.5 ^[73]
				4.03(<i>d</i>) ^[77]		
B phase						
DFT	3.14(<i>i</i>)	3.13(<i>i</i>)	3.15(<i>i</i>)	4.7(<i>i</i>) ^{*[12]}		3.9 ^[71] , 4.2 ^[72]
DFT-1/2	4.87(<i>i</i>)	4.88(<i>i</i>)	4.90(<i>i</i>)			4.5 ^[73]
L _{SR} phase						
DFT	1.61(<i>i</i>)	1.86(<i>i</i>)	1.74(<i>i</i>)		2.96 ^[78]	3.9 ^[71] , 4.2 ^[72]
DFT-1/2	2.61(<i>i</i>)	2.91(<i>i</i>)	2.82(<i>i</i>)			4.5 ^[73]
β_R phase						
DFT	1.94 (<i>i</i>)	1.98 (<i>i</i>)	1.96 (<i>i</i>)			3.9 ^[71] , 4.2 ^[72]
DFT-1/2	3.89 (<i>i</i>)	3.96 (<i>i</i>)	3.94 (<i>i</i>)			4.5 ^[73]
Pm phase						
DFT	2.37 (<i>i</i>)	2.38 (<i>i</i>)	2.37 (<i>i</i>)			3.9 ^[71] , 4.2 ^[72]
DFT-1/2	4.28 (<i>i</i>)	4.32 (<i>i</i>)	4.31 (<i>i</i>)			4.5 ^[73]
$Cmmm$ phase						
DFT	2.09 (<i>i</i>)	2.17 (<i>i</i>)	2.12 (<i>i</i>)			3.9 ^[71] , 4.2 ^[72]
DFT-1/2	4.00 (<i>i</i>)	4.10 (<i>i</i>)	4.06 (<i>i</i>)			4.5 ^[73]
γ phase (relaxed)						
DFT	2.26(<i>i</i>)	2.32(<i>i</i>)	2.26(<i>i</i>)	3.75, 4.51 ^{&[13]}		3.9 ^[71] , 4.2 ^[72]
DFT-1/2	4.17(<i>i</i>)	4.23(<i>i</i>)	4.21(<i>i</i>)			4.5 ^[73]
η phase						
						3.9 ^[71] , 4.2 ^[72]

DFT	2.22(i)	2.30(i)	2.25(i)	4.5 ^[73]
DFT-1/2	4.12(i)	4.24(i)	4.20(i)	

* PBEsol based HSE06 calculation. # screened exchange hybrid functional calculation.

& PBE0 hybrid functional calculation.

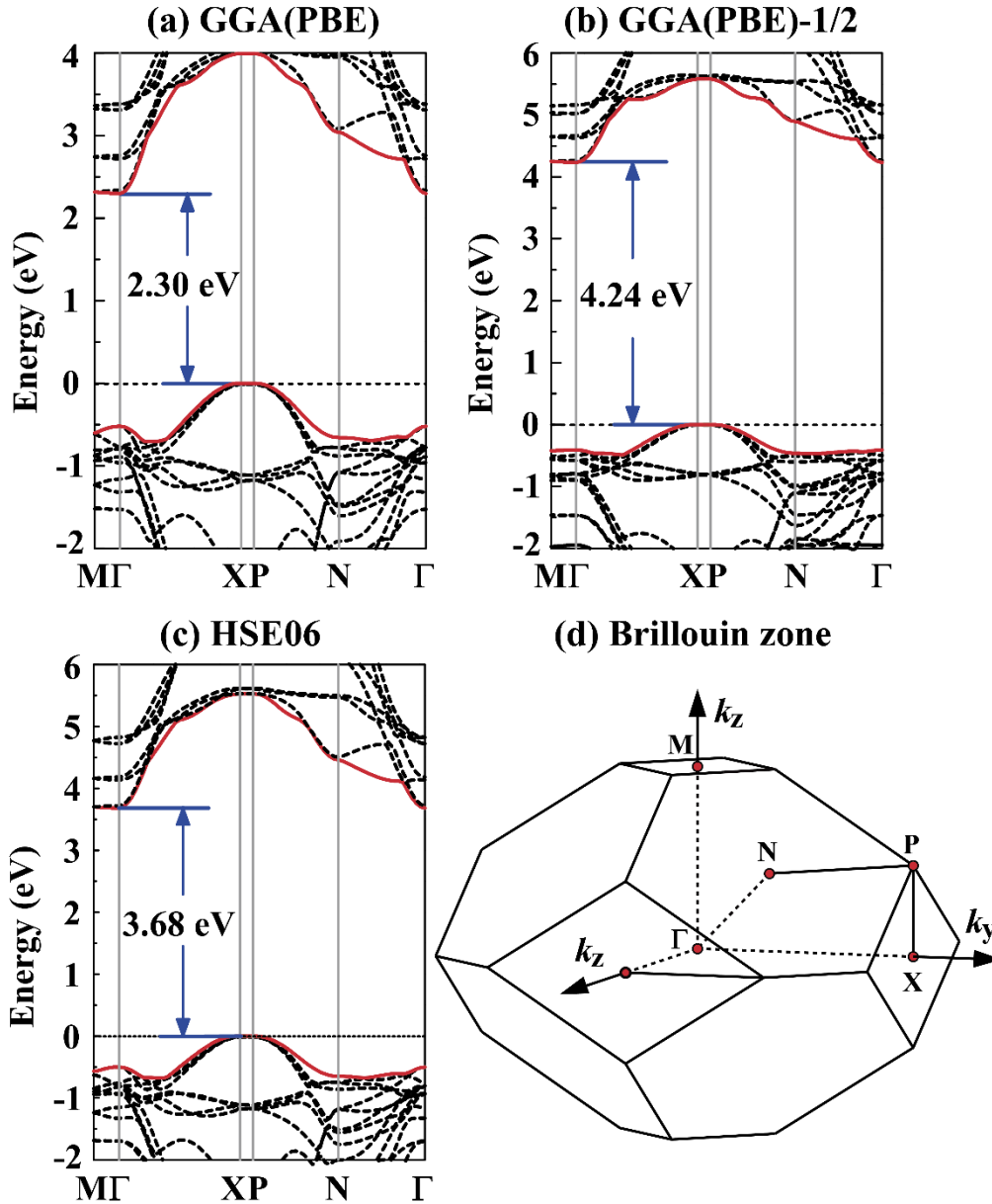


Figure 7. (a) Electronic band diagram of η -Ta₂O₅ calculated using GGA(PBE); (b) electronic band diagram of η -Ta₂O₅ calculated using GGA(PBE)-1/2; (c) electronic band diagram of η -Ta₂O₅ calculated using HSE06, with the PBE-optimized structure; (d) the first Brillouin zone of space group $I4_1/amd$.

The electronic structures of η -Ta₂O₅ are demonstrated in **Figure 7**, where the band

diagrams show indirect ($X-\Gamma$) band gaps of 2.30 eV and 4.24 eV according to GGA(PBE) and GGA(PBE)-1/2. The 4.24 eV indirect band gap is a reasonable value that recovers the electronic structure of L-Ta₂O₅ fairly well, and superior to the HSE06 band gap value of 3.68 eV, but the computational time of GGA-1/2 is typically less than 1.15 times the standard GGA calculation time for the same supercell.^[79] Hence, it is in principle possible to simulate a Ta₂O₅-based supercell with more than 500 atoms, without suffering from the band gap underestimation problem. The HSE06 band gap is slightly underestimated because its standard screening length for exact exchange is designed for moderate band gap semiconductors, while it is possible that insufficient exact exchange is mixed for insulators with band gaps greater than 4 eV. However, the morphologies of band structures in **Figure 7(b)** and **7(c)** are quite similar, supporting the validity of GGA-1/2 band structures.

In **Table 2** we list the calculated band gaps for other phases, where the representative GGA(PBE)-1/2 gap values indeed show great variability. For instance, the β_{AL} phase only demonstrates an indirect 1.85 eV band gap, followed by the hexagonal δ -phase which also shows a relatively narrow 2.56 eV band gap. On the contrary, the high pressure B-phase owns the largest 4.88 eV band gap. The band gaps calculated for most orthorhombic/monoclinic/tetragonal phases are close to 4 eV, including λ , β_R , Pm and $Cmmm$ phases. The low band gap for the L_{SR} phase stems from the existence of oxygen vacancy sites. Finally, compared with reported theoretical values in the literature, we find that the GGA-1/2 method predicts very similar data with the correct sequence of

band gaps among various model structures.

Band offset between Ta and Ta₂O₅

As Ta₂O₅ is an excellent candidate material for memristors, it is worthwhile to investigate its interfacial properties with respect to possible metal electrodes. As an application of the high symmetry η -Ta₂O₅ structure, we used the GGA-1/2 method to explore the electronic properties of the Ta/Ta₂O₅ interface. The structures of Ta and Ta₂O₅ were body-centered cubic and tetragonal $I4_1/amd$, respectively, but the mismatch of their lattice constants is as large as 17%. Yet, as the a/b lattice constants of both structures are less than 4 Å, we could reach a relatively good match by combining the $\sqrt{10} \times \sqrt{10}$ a - b surface of Ta and the $2\sqrt{2} \times 2\sqrt{2}$ a - b surface of Ta₂O₅, while keeping the total interfacial area for the supercell as low as 1.15 nm². The fully optimized atomic structures and the layer-decomposed local density of states are demonstrated in **Figure 8**. The contact of Ta/Ta₂O₅ has been shown to be Ohmic according to our GGA-1/2 calculation, since the Fermi level is aligned with the conduction band edge inside Ta₂O₅. The exact contact property of Ta/Ta₂O₅ was rarely reported in the literature, but recently Kim *et al.* assumed that the Ta/Ta₂O₅ interface points to Ohmic contact,^[80] which is consistent with our results.

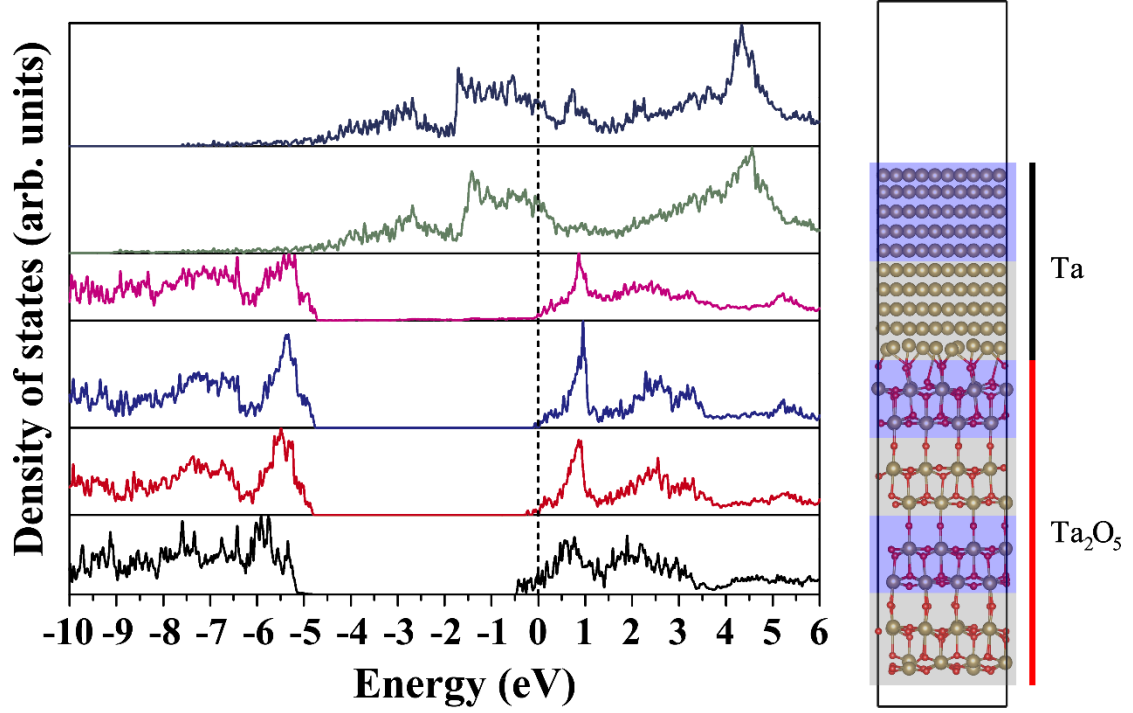


Figure 8. Layer-decomposed local density of states (LDOS) of our optimized Ta/Ta₂O₅ interface model, with the model structure and layer-decomposition scheme illustrated on the right. Each LDOS corresponds to a shaded layer following the same up-down sequence, and the Fermi level is set to zero energy.

IV. CONCLUSION

In summary, we find that the triclinic γ -phase of Ta₂O₅ is transformed into a much more symmetric $I4_1/amd$ structure (η -phase Ta₂O₅) during structural relaxation. Compared with various other Ta₂O₅ models, η -phase Ta₂O₅ has the lowest energy. Hence, both the high temperature α -phase and low temperature η -phase of Ta₂O₅ can be assigned the $I4_1/amd$ space group, but the α -phase is dynamically unstable at zero temperature. Using the GGA-1/2 self-energy correction method, the band gap of η -phase Ta₂O₅ is shown to be indirect (X- Γ) with a value of 4.24 eV. The high symmetry tetragonal model structure combined with the efficient GGA-1/2 method enables *ab initio* simulation of

Ta₂O₅-based devices. In particular, we confirm the Ohmic contact nature of Ta/Ta₂O₅ interface according to *ab initio* calculations, taking advantage of the simple structure of η-Ta₂O₅.

ACKNOWLEDGEMENTS

This work was financially supported by the MOST of China under Grant No. 2016YFA0203800, the National Natural Science Foundation of China under Grant No. 11704134 and 51732003, and the Fundamental Research Funds of Wuhan City under Grant No. 2017010201010106. L.R.C. Fonseca thanks the Brazilian agency CNPq for financial support under Grant No. 118485/2017-2.

REFERENCES

- [1] M. Satoh, H. Ishikawa, K. Amano, E. Hasegawa, and K. Yoshino, *Synth. Met.* **1995**, *71*, 2259.
- [2] C.-L. Wu, C.-H. Hsieh, G.-R. Lin, W.-C. Chi, Y.-J. Chiu, Y.-Y. Lin, Y.-J. Hung, M.-H. Shih, A.-K. Chu, and C.-K. Lee, *Ann. Phys.* **2016**, *529*, 1600358.
- [3] M. Hála, R. Vernhes, O. Zabeida, J.-E. Klemberg-Sapieha, and L. Martinu, *J. Appl. Phys.* **2014**, *116*, 213302.
- [4] E. Atanassova and A. Paskaleva, *Model. Negat. Bias Temp. Instab.* **2007**, *47*, 913.
- [5] M.-J. Lee, C. B. Lee, D. Lee, S. R. Lee, M. Chang, J. H. Hur, Y.-B. Kim, C.-J. Kim, D. H. Seo, S. Seo, U.-I. Chung, I.-K. Yoo, and K. Kim, *Nat. Mater.* **2011**, *10*, 625.
- [6] G.-S. Park, Y. B. Kim, S. Y. Park, X. S. Li, S. Heo, M.-J. Lee, M. Chang, J. H. Kwon, M. Kim, U.-I. Chung, R. Dittmann, R. Waser, and K. Kim, *Nat. Commun.* **2013**, *4*.
- [7] L. Goux, A. Fantini, Y. Y. Chen, A. Redolfi, R. Degraeve, and M. Jurczak, *ECS Solid State Lett.* **2014**, *3*, Q79.
- [8] H. Wu, X. Li, F. Huang, A. Chen, Z. Yu, and H. Qian, *Nanotechnology* **2015**, *26*, 035203.
- [9] A. Wedig, M. Luebben, D.-Y. Cho, M. Moors, K. Skaja, V. Rana, T. Hasegawa, K. K. Adepalli, B. Yildiz, R. Waser, and I. Valov, *Nat. Nanotechnol.* **2015**, *11*, 67.

- [10] B. Wang, K. H. Xue, H. J. Sun, Z. N. Li, W. Wu, P. Yan, N. Liu, B. Y. Tian, X. X. Liu, and X. S. Miao, *Appl. Phys. Lett.* **2018**, *113*, 183501.
- [11] N. C. Stephenson and R. S. Roth, *Acta Crystallogr. Sect. B* **1971**, *27*, 1037.
- [12] S. Pérez-Walton, C. Valencia-Balvín, A. C. M. Padilha, G. M. Dalpian, and J. M. Osorio-Guillén, *J. Phys. Condens. Matter* **2016**, *28*, 035801.
- [13] Y. Yang and Y. Kawazoe, *Phys Rev Mater.* **2018**, *2*, 034602.
- [14] L. Zhu, J. Zhou, Z. Guo, and Z. Sun, *J. Phys. Chem. C* **2016**, *120*, 2456.
- [15] S. Sathasivam, B. A. D. Williamson, A. Kafizas, S. A. Althabaiti, A. Y. Obaid, S. N. Basahel, D. O. Scanlon, C. J. Carmalt, and I. P. Parkin, *J. Phys. Chem. C* **2017**, *121*, 202.
- [16] X. Zhao and D. Vanderbilt, *Phys Rev B* **2002**, *65*, 233106.
- [17] A. S. Foster, F. Lopez Gejo, A. L. Shluger, and R. M. Nieminen, *Phys. Rev. B* **2002**, *65*, 174117.
- [18] J. X. Zheng, G. Ceder, T. Maxisch, W. K. Chim, and W. K. Choi, *Phys. Rev. B* **2007**, *75*, 104112.
- [19] D. Muñoz Ramo, A. L. Shluger, J. L. Gavartin, and G. Bersuker, *Phys. Rev. Lett.* **2007**, *99*, 155504.
- [20] K. McKenna, A. Shluger, V. Iglesias, M. Porti, M. Nafria, M. Lanza, and G. Bersuker, *Proc. 17th Bienn. Int. Insul. Films Semicond. Conf.* **2011**, *88*, 1272.
- [21] K.-H. Xue, P. Blaise, L. R. C. Fonseca, and Y. Nishi, *Phys. Rev. Lett.* **2013**, *110*, 065502.
- [22] K.-H. Xue, P. Blaise, L. R. C. Fonseca, G. Molas, E. Vianello, B. Traoré, B. D. Salvo, G. Ghibaudo, and Y. Nishi, *Appl. Phys. Lett.* **2013**, *102*, 201908.
- [23] K.-H. Xue, B. Traore, P. Blaise, L. R. C. Fonseca, E. Vianello, G. Molas, B. D. Salvo, G. Ghibaudo, B. Magyari-Kope, and Y. Nishi, *IEEE Trans. Electron Devices* **2014**, *61*, 1394.
- [24] S. R. Bradley, G. Bersuker, and A. L. Shluger, *J. Phys. Condens. Matter* **2015**, *27*, 415401.
- [25] J. Zhang, A. R. Oganov, X. Li, K.-H. Xue, Z. Wang, and H. Dong, *Phys. Rev. B* **2015**, *92*, 184104.
- [26] K.-H. Xue and X.-S. Miao, *J. Appl. Phys.* **2018**, *123*, 161505.
- [27] K.-H. Xue, H.-L. Su, Y. Li, H.-J. Sun, W.-F. He, T.-C. Chang, L. Chen, D. W. Zhang, and X.-S. Miao, *J. Appl. Phys.* **2018**, *124*, 024103.
- [28] W. Kohn and L. J. Sham, *Phys. Rev.* **1965**, *140*, A1133.
- [29] J. P. Perdew and W. Yue, *Phys Rev B* **1986**, *33*, 8800.

- [30] J. P. Perdew, K. Burke, and M. Ernzerhof, *Phys. Rev. Lett.* **1996**, *77*, 3865.
- [31] P. Hohenberg and W. Kohn, *Phys. Rev.* **1964**, *136*, B864.
- [32] J. Heyd, G. E. Scuseria, and M. Ernzerhof, *J. Chem. Phys.* **2003**, *118*, 8207.
- [33] L. Hedin, *Phys. Rev.* **1965**, *139*, A796.
- [34] Z.-H. Cui and H. Jiang, *J. Phys. Chem. C* **2017**, *121*, 3241.
- [35] H. Jiang, R. I. Gomez-Abal, P. Rinke, and M. Scheffler, *Phys Rev B* **2010**, *81*, 085119.
- [36] J. Lee, W. Lu, and E. Kioupakis, *Appl. Phys. Lett.* **2014**, *105*, 202108.
- [37] A. Reisman, F. Holtzberg, M. Berkenblit, and M. Berry, *J. Am. Chem. Soc.* **1956**, *78*, 4514.
- [38] N. C. Stephenson and R. S. Roth, *J. Solid State Chem.* **1971**, *3*, 145.
- [39] X. Q. Liu, X. D. Han, Z. Zhang, L. F. Ji, and Y. J. Jiang, *Acta Mater.* **2007**, *55*, 2385.
- [40] R. Moser, *Schweiz Miner. Petrogr Mitt* **1965**, *45*, 35.
- [41] Nobuzo Terao, *Jpn. J. Appl. Phys.* **1967**, *6*, 21.
- [42] G. M. Wolten and A. B. Chase, *Z. Für Krist.* **2010**, *129*, 365.
- [43] F. Izumi and H. Kodama, *J. Common Met.* **1979**, *63*, 305.
- [44] V. P. Filonenko and I. P. Zibrov, *Inorg. Mater.* **2001**, *37*, 953.
- [45] H.-U. Hummel, R. Fackler, and P. Remmert, *Chem. Ber.* **1992**, *125*, 551.
- [46] A. Fukumoto and K. Miwa, *Phys Rev B* **1997**, *55*, 11155.
- [47] H. Sawada and K. Kawakami, *J. Appl. Phys.* **1999**, *86*, 956.
- [48] L. A. Aleshina and S. V. Loginova, *Crystallogr. Rep.* **2002**, *47*, 415.
- [49] R. Ramprasad, *J. Appl. Phys.* **2003**, *94*, 5609.
- [50] S.-H. Lee, J. Kim, S.-J. Kim, S. Kim, and G.-S. Park, *Phys Rev Lett* **2013**, *110*, 235502.
- [51] J.-Y. Kim, B. Magyari-Köpe, K.-J. Lee, H.-S. Kim, S.-H. Lee, and Y. Nishi, *Phys. Status Solidi RRL – Rapid Res. Lett.* **2014**, *8*, 560.
- [52] G. Kresse and J. Furthmüller, *Phys. Rev. B* **1996**, *54*, 11169.
- [53] G. Kresse and J. Furthmüller, *Comput. Mater. Sci.* **1996**, *6*, 15.
- [54] D. M. Ceperley and B. J. Alder, *Phys. Rev. Lett.* **1980**, *45*, 566.

- [55] J. P. Perdew and A. Zunger, *Phys. Rev. B* **1981**, *23*, 5048.
- [56] J. P. Perdew, A. Ruzsinszky, G. I. Csonka, O. A. Vydrov, G. E. Scuseria, L. A. Constantin, X. Zhou, and K. Burke, *Phys. Rev. Lett.* **2008**, *100*, 136406.
- [57] P. E. Blöchl, *Phys. Rev. B* **1994**, *50*, 17953.
- [58] G. Kresse and D. Joubert, *Phys. Rev. B* **1999**, *59*, 1758.
- [59] J. P. Perdew and M. Levy, *Phys Rev Lett* **1983**, *51*, 1884.
- [60] L. J. Sham and M. Schlüter, *Phys Rev Lett* **1983**, *51*, 1888.
- [61] R. W. Godby, M. Schlüter, and L. J. Sham, *Phys. Rev. B* **1988**, *37*, 10159.
- [62] L. G. Ferreira, M. Marques, and L. K. Teles, *Phys. Rev. B* **2008**, *78*, 125116.
- [63] J. M. Soler, E. Artacho, J. D. Gale, A. García, J. Junquera, P. Ordejón, and D. Sánchez-Portal, *J. Phys. Condens. Matter* **2002**, *14*, 2745.
- [64] J.-H. Yuan, Q. Chen, L. R. C. Fonseca, M. Xu, K.-H. Xue, and X.-S. Miao, *J. Phys. Commun.* **2018**, *2*, 105005.
- [65] I. P. Zibrov, V. P. Filonenko, M. Sundberg, and P.-E. Werner, *Acta Crystallogr. Sect. B* **2005**, *56*, 659.
- [66] Y.-N. Wu, L. Li, and H.-P. Cheng, *Phys Rev B* **2011**, *83*, 144105.
- [67] W. Petter and F. Laves, *Naturwissenschaften* **1965**, *52*, 617.
- [68] F. Laves, R. Moser, and W. Petter, *Naturwissenschaften* **1965**, *52*, 617.
- [69] C. Valencia-Balvín, S. Pérez-Walton, G. M. Dalpian, and J. M. Osorio-Guillén, *Comput. Mater. Sci.* **2014**, *81*, 133.
- [70] H. Xu, D. Lee, J. He, S. B. Sinnott, V. Gopalan, V. Dierolf, and S. R. Phillpot, *Phys Rev B* **2008**, *78*, 174103.
- [71] W.-J. Chun, A. Ishikawa, H. Fujisawa, T. Takata, J. N. Kondo, M. Hara, M. Kawai, Y. Matsumoto, and K. Domen, *J. Phys. Chem. B* **2003**, *107*, 1798.
- [72] W. H. Knausenberger and R. N. Tauber, *J. Electrochem. Soc.* **1973**, *120*, 927.
- [73] C. Chaneliere, J. L. Autran, R. A. B. Devine, and B. Balland, *Mater. Sci. Eng. R Rep.* **1998**, *22*, 269.
- [74] Z.-H. Cui and H. Jiang, *J. Phys. Chem. C* **2017**, *121*, 3241.
- [75] S.-H. Lee, J. Kim, S.-J. Kim, S. Kim, and G.-S. Park, *Phys. Rev. Lett.* **2013**, *110*.

- [76] R. Nashed, W. M. I. Hassan, Y. Ismail, and N. K. Allam, *Phys Chem Chem Phys* **2013**, *15*, 1352.
- [77] Y. Guo and J. Robertson, *Appl. Phys. Lett.* **2014**, *104*, 112906.
- [78] J. Lee, W. Lu, and E. Kioupakis, *Appl. Phys. Lett.* **2014**, *105*, 202108.
- [79] K.-H. Xue, J.-H. Yuan, L. R. C. Fonseca, and X.-S. Miao, *Comput. Mater. Sci.* **2018**, *153*, 493.
- [80] W. Kim, S. Menzel, D. J. Wouters, Y. Guo, J. Robertson, B. Roesgen, R. Waser, and V. Rana, *Nanoscale* **2016**, *8*, 17774.